Describing the structural shape of melanocytic lesions

Tim Lee[a,b†], Stella Atkins[b], Richard Gallagher[a], Calum MacAulay[a], Andy Coldman[a], David McLean[c]

[a] BC Cancer Agency, Vancouver, BC, Cananda

[b] Simon Fraser University, Burnaby, BC, Canada

[c] Vancouver Hospital and Health Sciences Centre and University of BC, Vancouver, BC, Canada

ABSTRACT

This paper presents an automatic computer system for analysing the structural shape of cutaneous melanocytic lesion borders. The computer system consists of two steps: pre-preprocessing the skin lesion images and lesion border shape analysis. In the preprocessing step, the lesion border is extracted from the skin images after the dark thick hairs are removed by a program called DullRazor. The second step analyses the structural shape of the lesion border using a new measure called sigma-ratio. The new measure is derived from scale-space filtering technique with an extended scale-space image. When comparing the new measure with other common shape descriptors, such as compactness index and fractal dimensional, sigma-ratio is more sensitive to the structural protrusions and indentations. In addition, the extended scale-space image can be used to pinpoint the locations of the structural indentations and protrusions, the potential problem areas of the lesion.

Keywords: medical image analysis, melanoma, shape, border irregularity, scale space filtering

1. INTRODUCTION

Cutaneous malignant melanoma incidence has increased rapidly in the last three decades.[1] Early detection is important for the treatment process because the survival rate is inversely proportional to the thickness of the lesion.[2] To detect melanomas as early as possible, many countries promote self-screening programs using the guidelines such as the ABCD rule or the Seven-point checklist.[3-6] These guidelines are based on the clinical differences between benign melanocytic nevi and malignant melanomas: melanocytic nevi are often described as small oval lesions with uniform colour, while melanomas are large asymmetrical lesions with a jagged and scalloped border and different shades of colours.[7,8]

Among these features, the irregular shape of the lesion border, referred to as border irregularity, has been suggested as the most important factor for clinical diagnosis.[9] When examining the lesion border carefully, we discover two types of irregularities: the fine variation along the border and the global variation with structural protrusions and indentations. The latter type of irregularity is more significant in the diagnosis of melanomas.[10] The structural protrusions may suggest abnormal and excessive growth of cells along one direction, and structural indentations may suggest regression. Examining the structural border irregularity may reveal important histologic information about the lesion.

Recently, there have been studies analysing the lesion shape.[10-17] These studies applied the common shape descriptors such as compactness index[18] and fractal dimension[19] to measure the overall roughness of the lesion border. However, there are shortcomings with these two shape descriptors. They do not measure the structural protrusions and indentations directly and may produce unsatisfactory results. Cross et al.[14] reported a poor correlation between melanomas and fractal dimension and other Euclidean geometric parameters. We have been studying digitized skin images with the aim of developing a computer system to differentiate shapes of malignant melanomas from melanocytic nevi. This paper presents an automatic computer system with a new shape descriptor that is sensitive to structural irregularities. Furthermore the new system can also pinpoint the structural indentations and protrusions. The analysis consists of two major steps: preprocessing the images to obtain the lesion borders, then analysing the borders for a "malignancy factor".

2. MATERIAL

The skin images used in the paper were collected from the patients referred to the Pigmented Lesion Clinics in Vancouver, BC, Canada. Each colour skin image contains the R, G, and B components and has 486 x 512 pixels with spatial resolution of 25μm x 33μm. These images are captured by a hand-held CCD video microscopy camera with a 20 times magnification lens. The camera connects to a shoebox-sized main unit, which is further connected to the frame grabber in a personal

† Send correspondence to Tim Lee whose email address is tlee@bccancer.bc.ca.

computer. The main unit provides a white light source back to the camera using an optic fiber cable. The light source forms a ring within a hollow cylinder attached to the front of the camera. During the imaging session, the cylinder is in direct contact with the patient's body. Besides acting as a stabilizer for the camera against excessive lateral or vertical movement, the cylinder also provides a standard lighting environment and focal length. Because the hand-held camera is both small and light in weight, it can be moved around the patient's body easily to capture skin images.

3. STEP 1: PREPROCESSING

Before the images can be used for shape analysis, they are processed by two automatic programs. First, a program called DullRazor performs dark thick hair removal and then an automatic segmentation program extracts the lesion border.

3.1. DullRazor

Many skin images contain hairs. These hairs, especially the dark thick ones with a similar colour hue to the lesion, cause problems for the segmentation program because they occlude the lesion and, therefore, mislead the segmentation program. Of course, we could shave the hairs before the imaging session. However, shaving is uncomfortable and time consuming, particularly when we want to digitize multiple lesions from the same patient. Hence, we designed a computer program called DullRazor[20] to remove the dark hairs from the skin images prior to the segmentation program.

A summary of DullRazor is presented here as it has been discussed in detail elsewhere[20]. In the skin images, dark thick hairs appear as long and narrow structures with low intensity values compared to the nearby skin. DullRazor detects these low intensity structures by applying grayscale morphological closing operations in several directions. The maximum response from all directions is obtained to create a hair mask that identifies the location of hairs. Each possible pixel within the mask is further verified to ensure the mask is noise free. Then the corresponding hair pixels are replaced by the nearby non-hair pixels using binary interpolation. Finally, a 5 x 5 adaptive median filter smoothes all replaced pixels and the nearby pixels. DullRazor modifies only the hair pixels and their nearby pixels to reduce the alternation to a minimum. Fig. 1a shows a skin image covered by dark thick hairs, and Fig. 1b shows the hair mask computed by DullRazor and Fig. 1c shows the modified skin image with the hairs removed.

3.2. Automatic Segmentation

The removal of the dark thick hairs simplifies the segmentation process. The skin image now contains a lesion surrounded by normal skin. The normal skin has a uniform colour tone, while the lesion may contain different shades of colours. The segmentation process has been described in Ref. 21 and a brief summary is presented here.

The first step of the segmentation process is to smooth the R, G, and B component of image with a set of specially designed weighted median filters. These median filters remove the outliners and impulse noise. Then a coarse threshold range is determined for each component by analysing the component's histogram. For every intensity value within the threshold range, the distribution of the corresponding pixels is examined. These pixels are aggregated into two groups: lesion group and normal skin group. The normal skin group pixels are scattered around the entire image and appear as noise, while the lesion group concentrates together. We select the final threshold value that contains the largest lesion area with the acceptable amount of noise (normal skin). After a threshold value is selected for all components, a rule-based system is used to combine the segmentation results from the R, G, and B component and to clean up the noise pixels, i.e., the normal skin pixels. Because the melanocytic lesion has a high absorption for the short wavelength light spectrum, the lesion will have a very low intensity value in the B component and it is more stable for the segmentation process. Therefore, more weight is put on the B component. Fig. 2 shows the final segmentation results for Fig. 1a.

4. STEP 2: BORDER SHAPE ANALYSIS

Once the segmentation process is completed, we analyse the lesion border with a new border irregularity measure that is sensitive to structural protrusions and indentations. Furthermore, the new measure can pinpoint the location of the protrusions and indentations.

4.1. Curvature

The curvature of a curve provides much information. The magnitude is proportional to the amount of bending and the sign indicates concavity or convexity of the curve segment. For example, Fig. 3a displays a simple curve line with two protrusions and one overlapping indentation. Fig. 3b plots the corresponding curvature function. The local curvature extrema, labelled as A, B, C, D, and E, can be located by checking the zero-crossings of the first derivative of the curvature

function. (See Fig. 3c.) The local extrema correspond to the tips of the protrusions and indentations. For this paper, a protrusion is defined precisely as a curve segment that begins with a concave curvature extreme, following by a convex curvature extreme and ending with a concave extreme. Similarly, an indentation is defined as a curve segment that begins with a convex curvature extreme, following by a concave curvature extreme and ending with a convex curvature extreme. For instance, the two protrusions shown in Fig. 3a are delimited as the curve segment [A, B, C] and [C, D, E], while the indentation is delimited as [B, C, D]. We can apply the curvature operations described above to a lesion border, if the border is abstracted as a closed planar curve. Further simplification can be made by parameterization of the x and y coordinates into two linear functions x(t) and y(t), where t is the path length variable along the planar curve.[22] However, the curvature operation is a local operation that computes local curvature values.

4.2. Extended Scale-space Image

Convolution with a Gaussian filter is a well-known smoothing technique in computer vision to extract global structure. The scale-space theory showed that a Gaussian filter is the only convolution kernel that satisfies 'causality' property of filtering.[23] In other words, no new irregularities are generated as artifacts during a continuous smoothing process and irregularities are smoothed out gradually in a 'proper' order. Small protrusions and indentations disappear before larger ones. (See Fig. 4 for a demonstration of the Gaussian smoothing process. A lesion border is smoothed by an increasing σ.) Unfortunately, Gaussian smoothing also distorts the shape of the curve and the locations of any feature, such as the locations of the local curvature extrema. Scale-space theory solves the distortion problem by proposing a 2-D scale-space image.[22,24] The feature locations are recorded in the scale-space image as the curve is smoothed continuously. For the current application, the scale-space image needs to be extended from a binary image to a three-valued image to encode the local concavity or convexity of the curve segment. Such an extended scale-space image for the smoothing process illustrated in Fig. 4 is constructed and showed in Fig. 5. The y-axis of the image represents the smoothing scale that is denoted by Gaussian σ, and the x-axis represents the spatial position of the investigated feature, the local extreme positions of the curvature function. At any smoothing scale σ, the curvature function of the smoothed curve is computed and the zero-crossings of the first derivative of the curvature function are recorded as points on the image along with the concavity or convexity of the local curve segment. For example, at $\sigma = 30$, point A on the border of Fig. 4 corresponds to point A on Fig. 5. The lines formed by these points depict the evolution of the local curvature extrema as they are smoothed by an increasing σ. With the help of these lines, indentations and protrusions, as defined previously in this paper, can be detected for all smoothing scales. For instance, in Fig. 5, one of the indentations begins from the convex curvature extreme line marked with B, to the concave curvature extreme line C, and ends at the convex curvature extreme line D. This indentation emerges at $\sigma = 37$ when all nested smaller irregularities have been smoothed out, and it ends at $\sigma = 93$ when the concave curvature extreme line C converts to a convex extreme.

There is another interesting difference in our extended 3-value scale-space image from the ordinary scale-space images: some of the lines in the image may not close off at the top. During the smoothing process, the concave extrema disappear in two fashions. Some of them disappear with a neighbouring convex extreme and hence produce a closed line such as the one marked as E in Fig. 5. Other concave extrema may convert to a convex extreme and produce a line extending out of the image, such as line F in Fig. 5. When all concave extrema disappear, i.e., the smoothed curve becomes an oval shape, the smoothing process can be terminated.

4.3. A New Shape Descriptor, Sigma-ratio

The final σ value required in the above smoothing process is a good measurement for the overall ruggedness of the lesion curve. For example, the smoothing process shown in Fig. 4 and 5 has a final σ value of 93. However, this measurement depends on the length of the lesion border and the lengths of the irregularities along the border. When the lesion is enlarged, the absolute final σ value is increased accordingly. We should normalize the measurement to make it scale invariant so that it can be used for lesion borders with different lengths. Hence, a sigma-ratio is defined as a ratio of the final σ value over the border length.[‡] The normalization yields a relative final σ level value that is independent of the length of the border.

4.4. Compare Sigma-ratio with Compactness Index and Fractal Dimension

In order to experiment with the new measure, sigma-ratio, we preprocessed ten typical lesion images from our database and computed the compactness index, fractal dimension and sigma-ratio for each lesion border. The ten lesion borders are shown in Fig. 6. The compactness index is the ratio of the area of the circle with the same circumference as the lesion over the area

[‡] Because the final σ level is a linear function of the 1-D Gaussian kernel length, the current implementation divides the kernel length by the entire border length.

of the lesion[18] and the box-counting method is used to compute the fractal dimension.[13] The process to compute sigma-ratio is described in section 4.1 to 4.3. All results are tabulated in Table 1.

Comparing the rankings of a lesion border in the three measurements helps to analyze the results in Table 1. The ten lesion borders are sorted by the corresponding measurements and are re-plotted in Fig. 7 to Fig. 9. It is interesting to note that the compactness index and fractal dimension have a similar ranking; three of ten test borders are ranked in the same positions. These borders are obj6, obj4, and obj1 and their corresponding rankings are 3rd, 6th, and 10th. Furthermore, the Spearman's rank correlation coefficient for these two measurements is 0.939. (See Table 2.) The correlation coefficient of 1 implies a perfect positive correlation, and a coefficient of 0 implies that the measurements are not correlated. A coefficient of 0.939 confirms a high correlation between the ranking of the compactness index and fractal dimension. On the other hand, the ranking for sigma-ratio looks different from the other two measurements. The Spearman's rank correlation coefficient achieves the same low value of 0.697 for sigma-ratio and other two measurements. (See Table 2.)

Carefully examining the results in Fig. 6 to Fig. 9, we notice that the compactness index and fractal dimension are sensitive to local irregularities and they fail to recognize the existence of the structural protrusions and indentations. For example, the test borders obj2, obj4 and obj7 have distinct shapes. The test border obj2 has a relatively smooth border with a structural protrusion at the top. The test border obj4 has many local irregularities with no structural protrusion and indentation, and the test border obj7 has a prominent structural protrusion and indentation at the bottom. These borders are ranked in a similar order by the compactness index and fractal dimension. For compactness index, these three borders are ranked as 1st, 6th, and 5th, respectively, with the actual values 2.521, 4.810 and 4.159. The rankings for the fractal dimension are 2nd, 6th, and 4th with the values as 1.075, 1.151 and 1.115, respectively. In spite of lacking any structural irregularity, obj4 achieves the highest ranking (6th) among these three borders for the compactness index and fractal dimension. Furthermore, the structural irregularities in obj2 and obj7 are ignored by these two measurements. Another way to view the problem is that the compactness index and fractal dimension calculate an 'average' value that can be skewed easily if the variance of the border ruggedness is large. The smoothed portion of the lesion border may dampen the final measurement for obj2 and obj7. On the contrary, the sigma-ratios for these three borders are 0.534, 0.445, and 0.708, respectively. The border obj4 has the lowest value and it ranks 4th. The border obj7 with prominent irregularities obtains the highest ranking of 7th. Sigma-ratio assigns a proper order for these three borders based on the structural irregularities.

4.5. Discussion

We performed sensitive tests on the new measure using phantom images. Fig. 10 shows one of the images and its smoothing process. It is a circle with a very narrow and long indentation in the right side of the circle. Since dark thick hairs are presented in many skin images, any long hair missed by the pre-processing step may mimic a long and narrow indentation. However, this kind of structure has a very high sigma-ratio of 0.966. Fortunately, only hairs longer than the largest protrusion or indentation will have a severe impact on the sigma-ratio. The shorter hairs will have a minimal effect. In any situation, this phantom exposes the importance of hair removal in the preprocessing step.

Another concern of the sigma-ratio is the non-linearity of the smoothing process. As demonstrated by Fig. 4 and Fig. 10, there is more smoothing power when σ is small. The normalization will not be able to correct the non-linearity problem.

An advantage of using this method to generate a new measure for the structural shape is that we can identify the location of protrusions and indentations. Especially, the last protrusion or indentation to be smoothed out is usually the most prominent irregularity and represents the potential problem area. This irregularity can be tracked by the extended scale-space image such as the one showed in Fig. 5. The lines formed by the curvature extrema depict the evolution of the irregularities as they are smoothed by an increasing scale. Tracking these lines from coarse-to-fine can map the irregularity back to the original non-smoothed curve. For example, the last indentation to be smoothed out in Fig. 5 is marked by the lines B, C and D. Following these lines, the location of the most prominent indentation is pinpointed and is shown in Fig. 11. The capability of locating the potential problem areas will make the new descriptor an attractive tool for physicians.

5. CONCLUSION

We have presented a computer system that processes a skin image and analyses the structural irregularity along the melanocytic lesion border. A new measure, called the sigma-ratio, is introduced. Based on an extended scale-space image, the sigma-ratio shows promising results as a structural shape descriptor. Unlike the common shape descriptors such as compactness index and fractal dimension, sigma-ratio is sensitive to the structural protrusions and indentations. Furthermore, the method to estimate the sigma-ratio can be extended to locate the irregularities along the lesion border. This feature may be useful to indicate potential problem areas. Further studies are underway to make the new measure a useful shape descriptor for border irregularity.

ACKNOWLEGEMENTS

This work was supported in part by a BC Health Research Foundation grant #142(97-2).

REFERENCES

1. B. K. Armstrong and D. R. English, "Cutaneous malignant melanoma," in *Cancer Epidemiology and Prevention*, D. Schottenfeld and J. F. Fraumeni Jr., eds., pp. 1282-1312, Oxford University Press, New York, 1996.
2. C. M. Balch, A. Houghton, and L. Peters, "Cutaneous melanoma," in *Cancer Principles and Practice of Oncology*, V. T. DeVita Jr., S. Hellman, and S. A. Rosenberg, eds., pp. 1499-1542, J. B. Lippincot Company, Philadelphia, 1989.
3. J. K. Rivers and R. P. Gallagher, "Public education projects in skin cancer - experience of the Canadian Dermatology Association," *Cancer* **75**(2 Suppl), pp. 661-666, 1995.
4. H. K. Koh, L. A. Norton, A. C. Geller, T. Sun, D. S. Rigel, D. R. Miller, R. G. Sikes, K. Vigeland, E. U. Bachenberg, P. A. Menon, F. S. Billon, G. Goldberg, D. A. Scarborough, W. M. Ramsdell, V. A. Muscarella, and R. A. Lew, "Evaluation of the American Academy of Dermatology's National Skin Cancer Early Detection and Screening Program," *J Am Academy of Dermatology* **34**, pp. 971-978, 1996.
5. H. Pehamberger, M. Binder, S. Knollmayer, and K. Wolff, "Immediate effects of a public education campaign on prognostic features of melanoma," *J Am Academy of Dermatology* **29**, pp. 106-109, 1993.
6. R. M. MacKie, "Melanoma prevention and early detection," *British Medical Bulletin* **51**, pp. 570-583, 1995.
7. J. K. Rivers. Melanoma. *Lancet* **347**, pp. 803-807, 1996.
8. J. C. Maize and A. B. Ackerman, *Pigmented Lesions of the Skin*, Lea & Febiger, Philadelphia, 1987.
9. M. Keefe, D. Dick, and R. Wakeel, "A study of the value of the seven-point checklist in distinguishing benign pigmented lesions from melanoma," *Clinical Experimental Dermatol* **15**, pp.167-171, 1990.
10. E. Claridge, P. N. Hall, M. Keefe, and J. P. Allen, "Shape analysis for classification of malignant melanoma," *J Biomed Eng* **14**, pp. 229-234, 1992.
11. E. Claridge, J. D. Morris Smith, and P. N. Hall, "Evaluation of border irregularity in pigmented skin lesions against a consensus of expert clinicians," in *Medical Image Understanding and Analysis*. Leeds, UK, 1998.
12. O. Colot, R. Devinoy, A. Sombo, and D. de Brucq, "A color image processing method for melanoma detection," in *Proc. of the First International Medical Imaging Computing and Computer-Assisted Intervention*, pp. 562-569,1998.
13. V. Ng and T. Lee, "Measuring border irregularities of skin lesions using fractal dimensions". *Proc. SPIE* **2898**, pp. 64-72,1996.
14. S. S. Cross, A. J. McDonagh, T. J. Stephenson, D. W. Cotton, and J. C. Underwood, "Fractal and integer-dimensional geometric analysis of pigmented skin lesions," *Am J Dermatopathol* **17**, pp. 374-378, 1995.
15. F. Ercal, A. Chawla, W. V. Stoecker, H. C. Lee, and R. Moss. "Neural network diagnosis of malignant melanoma from color images," *IEEE Trans Biomed Eng* **41**, pp. 837-845, 1994.
16. R. White, D. S. Rigel, and R. Friedman, "Computer applications in the diagnosis and prognosis of malignant melanoma," *Dermatologic Clinics* **9**, pp. 695-702, 1992.
17. J. E. Golston , W. V. Stoecker, R. H. Moss, and I. P. S. Dhillon. "Automatic detection of irregular borders in melanoma and other skin tumors," *Computerized Medical Imaging and Graphics* **16**, pp.199-203, 1992.
18. M. Sonka, V. Hlavac, and R. Boyle, *Image, Processing, Analysis and Machine Vision*, Chapman & Hall, 1995.
19. B. B. Mandelbrot, *The Fractal Geometry of Nature*, W.H. Freeman and Co., New York, 1982.
20. T. Lee, V. Ng, R. Gallagher, A. Coldman, and D. McLean, "DullRazor: A software approach to hair removal from images," *Comput Biol and Med* **27**, 533-543, 1997.
21. T. Lee, V. Ng, D. McLean, A. Coldman, R. Gallagher, and J. Sale. "A multi-stage segmentation method for images of skin lesions," *Proc. of IEEE Pacific Rim Conference on Communications, Computers and Signal Processing*, pp. 602-605, 1995.
22. F. Mokhtarian and M. Mackworth, "Scale-based description and recognition of planar curves and two-dimensional shapes," *IEEE Trans on Pattern Analysis and Machine Intelligence* **8**, 34-43, 1986.
23. T. Lindeberg, *Scale-space theory in computer vision*, Kluwer Academic Publishers, Boston, 1994.
24. A.P. Witkin AP, "Scale space filtering," *Proceedings of the 8th International Joint Conference of Artificial Intelligent* 1019-1022, 1983.

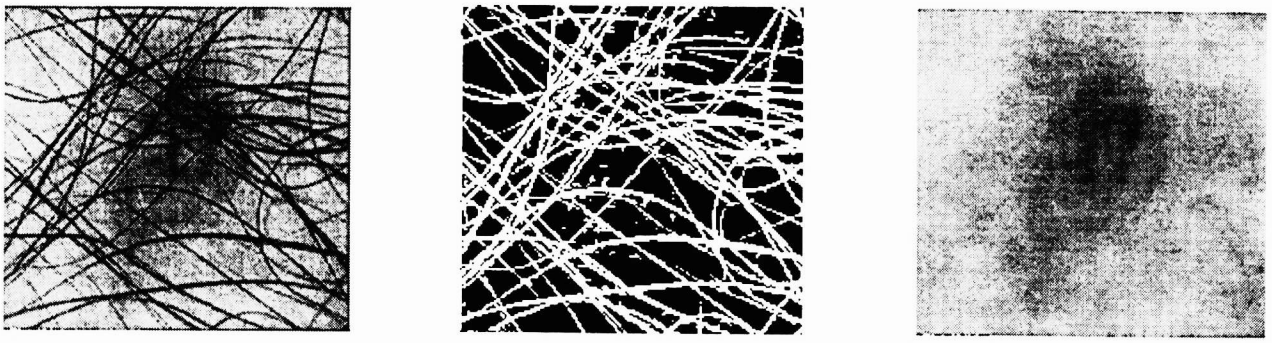

(a) (b) (c)

Figure 1. (a) A melanocytic lesion image covered by dark thick hairs. (b) The hair mask determined by the program DullRazor. (c) the lesion image with hairs removed.

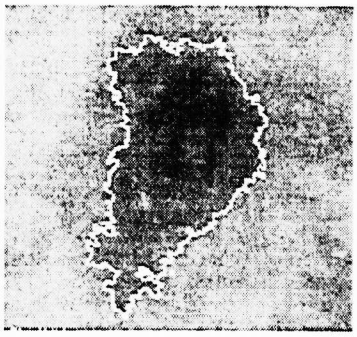

Figure 2. The segmentation result of the melanocytic lesion image showed in Fig. 1a.

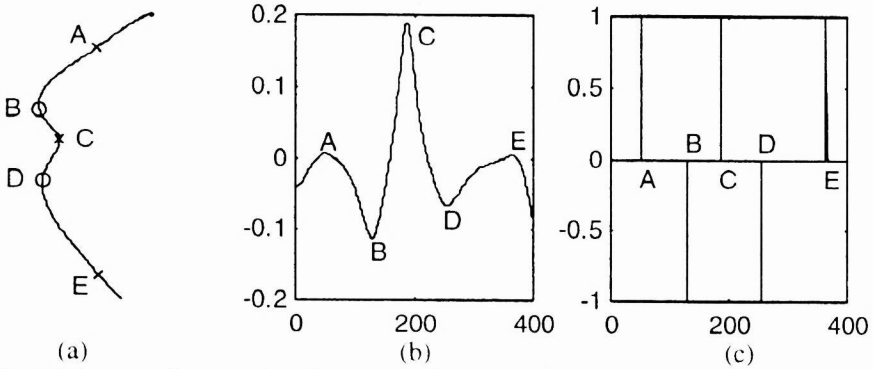

(a) (b) (c)

Figure 3. (a) A curve line running from top to bottom with two protrusions and one overlapping indentation: the protrusions are denoted by the curve segment [A B C] and [C D E], and the indentation is denoted by the curve segment [B C D]. (b) The curvature function of the curve line showed in a. The local extrema A, B, C, D, and E correspond to the tips of the protrusions and indentations. (c) The zero-crossing of the first derivative of the curvature function: these zero-crossing points mark the locations of the local extrema of the curvature function. The zero-crossing locations and signs are the feature points of the extended scale-space image.

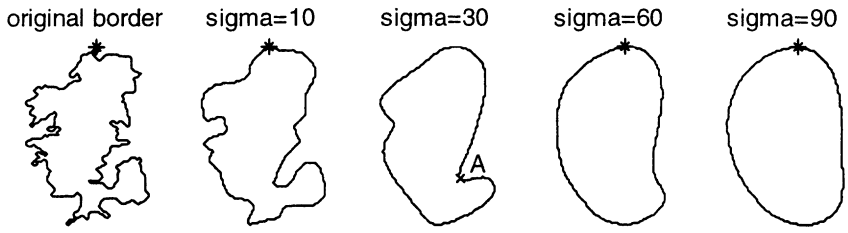

Figure 4. A melanocytic lesion border is continuously smoothed by a Gaussian filter with an increasing sigma (σ). The first plot is the original border. The other plots show the smoothed border with the corresponding σ denoted on the top of the plot. The beginning point of the parameterization is marked by '*' and the parameterization is done in the counterclockwise direction. For $\sigma = 30$, the point A corresponds to the point A in Fig. 5.

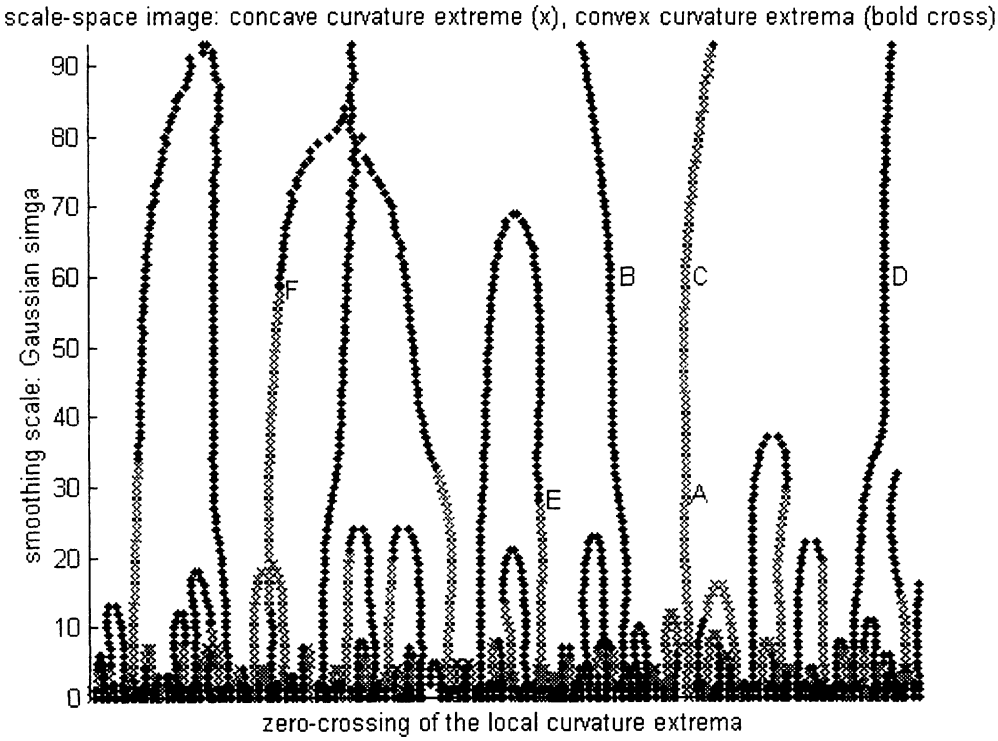

Figure 5. The extended scale-space image of the Gaussian smoothing process showed in Fig. 4. The point A corresponds to the point A in Fig. 4. The lines B, C, and D depict the evolution of an indentation during the smoothing process.

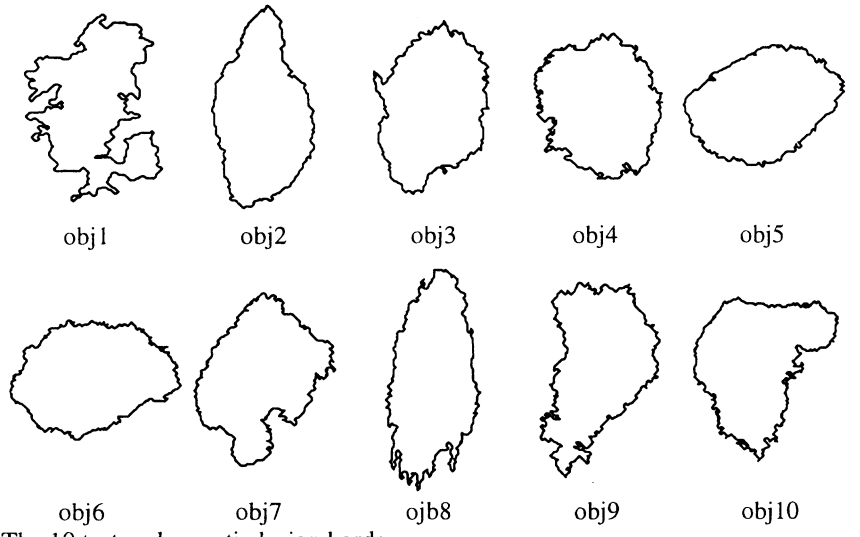

Figure 6. The 10 test melanocytic lesion borders.

Table 1. Compactness index, fractal dimension and sigma-ratio for the test objects

	Compactness index	Fractal dimension	Sigma-ratio
obj1	9.292	1.264	0.871
obj2	2.521	1.075	0.534
obj3	3.251	1.120	0.398
obj4	4.810	1.151	0.445
obj5	2.549	1.071	0.254
obj6	3.250	1.084	0.357
obj7	4.159	1.115	0.708
obj8	5.589	1.180	0.480
obj9	6.562	1.172	0.605
obj10	5.758	1.189	0.815

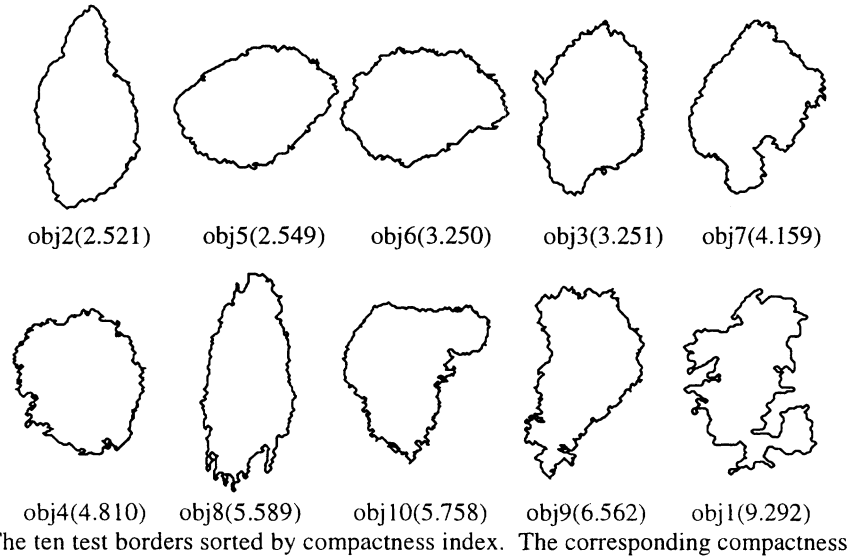

Figure 7. The ten test borders sorted by compactness index. The corresponding compactness indexes are showed inside the parentheses.

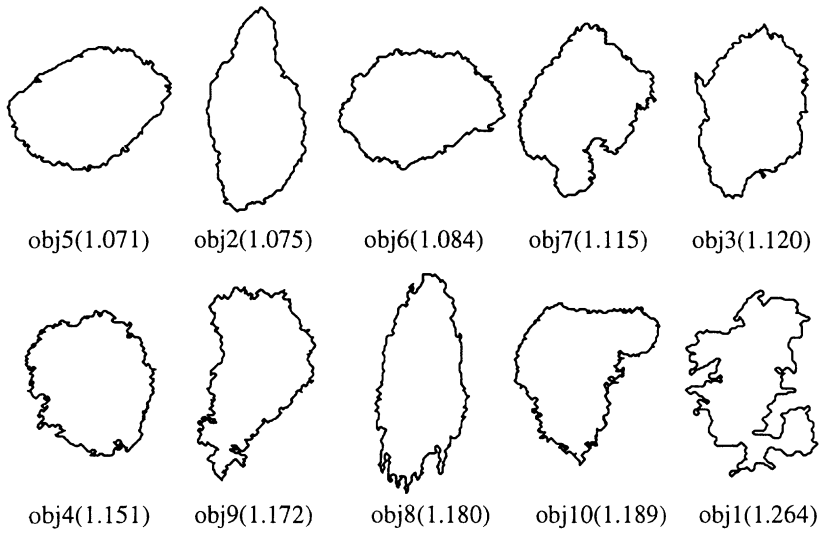

Figure 8. The test borders sorted by fractal dimension. The corresponding fractal dimensions are showed inside the parentheses.

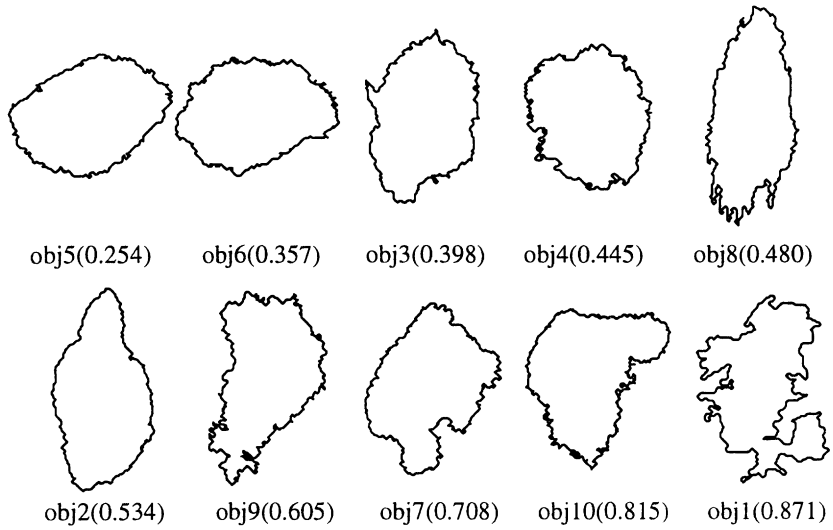

Figure 9. The tested borders sorted by sigma-ratio. The corresponding sigma-ratios are showed inside the parentheses.

Table 2. The Spearman's rank correlation coefficients for compactness index, fractal dimension and sigma-ratio of the test lesion borders.

	Compactness index	Fractal dimension	Sigma-ratio
Compactness index	1.0	0.939	0.697
Fractal dimension	0.939	1.0	0.697
Sigma-ratio	0.697	0.697	1.0

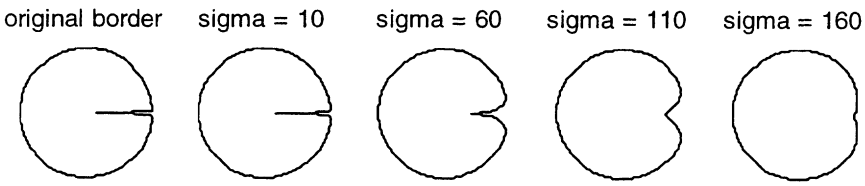

Figure 10. The Gaussian smoothing process for a phantom image. It is a circle with a long and narrow indentation in the right hand side.

Figure 11. The most prominent indentation on the malnaocytic lesion border, showed in Fig. 4, is highlighted. The indentation is located by a coarse-to-fine tracking of the extended scale-space image. This indentation is also the last irregularity to be smoothed out during the Gaussian smoothing process showed in Fig. 5.